JTTEE5 16:627–633
DOI: 10.1007/s11666-007-9087-7
1059-9630/$19.00 © ASM International

Numerical Study of Combination Parameters for Particle Impact Velocity and Temperature in Cold Spray

H. Katanoda, M. Fukuhara, and N. Iino

(Submitted March 1, 2007; in revised form July 16, 2007)

Numerical simulations of gas/particle flows of cold spray are performed for N_2 and He, respectively, to investigate the usefulness of the two material-independent combination parameters derived from the equations of particle motion and temperature. The first combination parameter is the particle-diameter multiplied by the material density, which governs the particle velocity. The second one is the squared particle-diameter multiplied by the material density and specific heat, which affects the particle temperature. In the numerical simulation, the materials of the spray particle selected are WC-12Co, Cu and Ti. The numerical results show that the maximum impact velocity of particle is obtained, when the first combination parameter takes specific value regardless of the material type. Furthermore, it is shown that the particle diameter and its temperature corresponding to the maximum impact velocity can be graphically estimated by using the two combination parameters for any powder-materials normally used for the thermal spray.

Keywords cold spray, particle impact-velocity, numerical simulation, gasdynamics

1. Introduction

As indicated by many experimental and numerical work of cold spray (Ref 1-4), the spray particle is required to have a higher impact velocity over a material-dependent critical velocity to be deposited on a substrate. Since the critical velocity depends on the particle temperature at impact, the particle velocity and particle temperature are two of the most important parameters. In the research on cold spray, we could predict the particle velocity and temperature by numerical simulation. From the powder-material point of view, the particle velocity depends on the material density, and the particle temperature depends on the material density as well as the specific heat. Since the density and specific heat varies from one material to another, we normally need to simulate the particle velocity and temperature for each powder-material independently (Ref 5).

This article is an invited paper selected from presentations at the 2007 International Thermal Spray Conference and has been expanded from the original presentation. It is simultaneously published in *Global Coating Solutions, Proceedings of the 2007 International Thermal Spray Conference*, Beijing, China, May 14-16, 2007, Basil R. Marple, Margaret M. Hyland, Yuk-Chiu Lau, Chang-Jiu Li, Rogerio S. Lima, and Ghislain Montavon, Ed., ASM International, Materials Park, OH, 2007.

H. Katanoda, M. Fukuhara, and **N. Iino**, Department of Mechanical Engineering, Kagoshima University, 1-21-40 Korimoto, Kagoshima, 890-0065, Japan. Contact e-mail: katanoda@mech.kagoshima-u.ac.jp.

Nomenclature

A_p	Projected area of particle
A_s	Surface area of particle
c_d	Drag coefficient of particle
c_p	Specific heat of gas at constant pressure
C	Specific heat of the particle
d_p	Particle diameter
d_p^*	Particle diameter at maximum impact-velocity
f_{prop}	Correction factor for thermal boundary-layer
k_g	Thermal conductivity of gas
m_p	Mass of particle
M_g	Gas Mach number
M_p	Particle Mach number
N_u	Nusselt number
P_r	Prandtl number of gas
Re_p	Particle Reynolds number
T_f	Film temperature
T_g	Gas temperature
T_p	Particle temperature
T_p^*	Particle temperature at maximum impact-velocity
u_g	Gas velocity
u_p	Particle velocity
u_{pi}	Particle impact-velocity
u_{pi}^*	Maximum particle impact-velocity
x	Axial distance along center line from nozzle exit

Greek Symbols

α	Heat transfer coefficient
γ	Specific heat ratio
μ_g	Gas viscosity
ρ_g	Gas density
ρ_p	Particle density

From the theoretical point of view, however, we can recognize two parameters which combine particle diameter and material properties. One is particle-velocity related parameter, which is the particle diameter multiplied by particle density (Ref 6), as in the equation of particle motion. The other one is, particle-temperature related parameter, which is the squared particle-diameter multiplied by the particle density and specific heat, as in the equation of particle energy.

This article investigates the particle velocity and temperature of cold spray for a wide range of both diameters and material properties of particle by numerical simulation. When the simulated particle impact-velocity is plotted against the particle-velocity related parameter, the distributions of the particle impact velocity are almost identical regardless of the material type. This is also true for the particle impact-temperature against the particle-temperature related parameter. In addition, the maximum impact velocity of particle, and corresponding temperature and diameter for any powder-material is graphically predicted by using numerical data for the specific powder-material. These results will improve our understanding of both acceleration and heating processes of particle in cold spray.

2. Numerical Methods

2.1 Gas Flow

The assumptions used in the present computational fluid dynamics (CFD) model are listed as follows:

(1) The gas flow is two-dimensional axisymmetric.
(2) The gas is thermally perfect and calorically perfect.
(3) The gas species inside and outside the nozzle is the same.
(4) The momentum transfer and heat transfer from the particle to the gas flow are neglected.

The above assumptions are normally used in the CFD model of the cold spray. The governing equations of the gas flow are given by the two-dimensional axisymmetric, time-dependent Navier-Stokes equations along with the k-ε turbulence model. The governing equations are solved sequentially in an implicit, iterative manner using a finite difference formulation. The governing equations are solved with the third-order, upwind, total variation diminishing scheme (Ref 7). The nitrogen and helium were used as a working gas independently in the CFD model. For N_2 and He, the stagnation pressure p_{os} and temperature T_{os} upstream of the nozzle were set at the same values of 3 MPa and 572 K, respectively. The atmospheric condition was set outside the nozzle as an initial condition.

Figure 1 shows an axisymmetric nozzle used in the CFD model. The nozzle has a throat diameter of 2 mm, an exit diameter of 7 mm, and a conically diverging length of 100 mm. The distance from the nozzle exit to the substrate

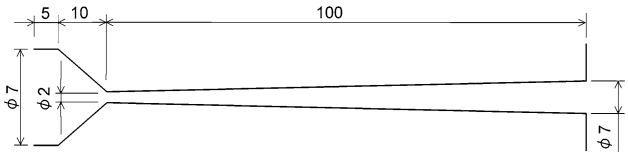

Fig. 1 Nozzle geometry (unit:mm)

is 10 mm. The size of the computational grid used in this simulation is 150×40 grids inside the nozzle, and 60×90 grids outside the nozzle. This grid size was found to be enough to obtain an almost mesh-size-independent solution; the finer computational grids, 230×60 and 90×135 for inside and outside the nozzle, respectively, showed negligible change in the gas velocity along the center line.

The steady one-dimensional isentropic theory (Ref 8) calculates the Mach number of the gas flow at the nozzle exit, the design Mach number M_d, of 4.15 for N_2. According to the theories of steady one-dimensional isentropic flow and normal shock wave (NSW), the M_d = 4.15 nozzle discharging N_2 gas generates an over-expanded flow at p_{os} = 3 MPa. In this case, we theoretically expect that the flow separates from the nozzle inner-wall by shock-wave/boundary-layer interaction (Ref 9). The similar flow pattern is also expected for the He case.

2.2 Particle Flow

The following assumptions are used to simulate the particle velocity and temperature to simplify the computation.

(1) The particles are spherical in shape.
(2) The particles travel along the nozzle axis.
(3) The interaction between the particles is negligible.
(4) The particle is accelerated by only gasdynamic drag force.
(5) The particle is heated by the gas through heat transfer.
(6) The temperature inside the particle is uniform.

Then, the equation of particle motion is written as;

$$m_p u_p \frac{du_p}{dx} = \frac{1}{2} c_d \rho_g (u_g - u_p) \cdot |u_g - u_p| A_p \qquad \text{(Eq 1)}$$

where x is the axial distance along the center line from the nozzle exit, ρ_g the gas density, u_g the gas velocity, m_p the mass of the particle, u_p the particle velocity, A_p the projected area of the particle, c_d the drag coefficient of the particle, respectively. The value of c_d was calculated by using a database made from the experimental data (Ref 10), along with a correction given by Eq 2 due to high temperature of the gas (Ref 11).

$$c_d = c_{d,exp} f_{prop}^{-0.45} \qquad \text{(Eq 2)}$$

where $c_{d,exp}$ is the drag coefficient obtained from the database, f_{prop} the correction factor given by Eq 9 later in this section.

The particle temperature can be calculated by the following equation;

$$m_p C u_p \frac{dT_p}{dx} = \alpha \cdot (T_g - T_p) \cdot A_s \quad \text{(Eq 3)}$$

where T_g is the gas temperature, T_p the particle temperature, C the specific heat of the particle, A_s the surface area of the particle, α the heat transfer coefficient which can be given as;

$$\alpha = k_{g,f} N_u / d_p \quad \text{(Eq 4)}$$

Here, N_u is the Nusselt number, k_g the thermal conductivity of the gas, d_p the particle diameter. The subscript f in Eq 4 means the value at the film temperature, T_f, defined as;

$$T_f = (T_g + T_p)/2 \quad \text{(Eq 5)}$$

The Nusselt number, N_u, in Eq 4 was computed by Ranz-Marshall correlation along with the correction factors (Ref 11).

$$N_u = \left(2 + 0.6 Re_p^{1/2} P_r^{1/3}\right) \cdot \left(\frac{c_p}{c_{p,w}}\right)^{0.38} f_{prop}^{0.6} \quad \text{(Eq 6)}$$

where c_p is the specific heat of the gas at constant pressure, and the subscript w indicates the surface of the particle. In Eq 6, the particle Reynolds number Re_p and the Prandtl number of the gas P_r are defined as;

$$Re_p \equiv \rho_{g,f} d_p |u_g - u_p| / \mu_{g,f} \quad \text{(Eq 7)}$$

$$P_r \equiv \mu_{g,f} c_{p,f} / k_{g,f} \quad \text{(Eq 8)}$$

where μ_g is the gas viscosity. The factors f_{prop} and f_{Kn} in Eq 6 represent the effect of variation in the gas temperature in the boundary layer on the particle surface and non-continuum effect, respectively. They are given as follows (Ref 11);

$$f_{prop} = \frac{\rho_g \mu_g}{\rho_{g,w} \mu_{g,w}} \quad \text{(Eq 9)}$$

The particle velocity and temperature were determined from a step-wise integration of Eq 1 and 3, respectively.

The powder-materials used in this simulation are WC-12Co, Cu and Ti, covering large to small material density and specific heat, as shown in Table 1. The range of the particle diameter is 0.1-30 μm for each material.

Table 1 Powder material

Material	WC-12Co	Cu	Ti
Density kg/m^3	14,320	8,960	4,510
Specific heat J/(kg K)	295	383	528

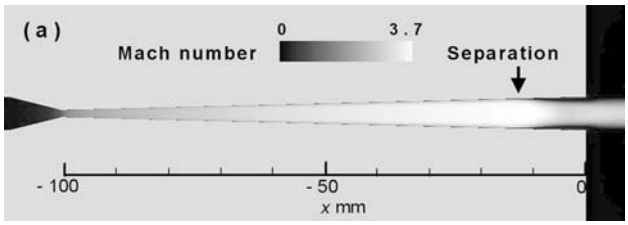

Fig. 2 Mach number contour for N_2 gas

3. Results and Discussion

3.1 Gas/Particle Flows

The simulated Mach number contour for N_2 gas is shown in Fig. 2. The axial distance measured from the nozzle exit, x, is shown in the bottom side of the figure. Figure 2 shows that the gas flow is accelerated to supersonic flow through the throat in the downstream direction. Then, the Mach number reaches the maximum value of $M_g = 3.7$ at $x \sim -10$ mm, around where the flow separates from the nozzle-wall, as was theoretically predicted in the previous chapter. The Mach number right before the NSW outside the nozzle is 2.8.

Figure 3a shows the velocities of the N_2 gas and 10 μm-Cu particle on the center line. The gas sharply accelerates through the nozzle throat, and then it gradually accelerates until the flow separates from the wall at $x \sim -10$ mm. After exiting the nozzle, the gas flow is suddenly decelerated through the NSW at $x = 9$ mm. The 10 μm-Cu particle is propelled by the N_2 gas, and then, it impinges the substrate at 631 m/s.

Figure 3b shows the velocities of the He gas and 10 μm-Cu particle on the center line. The He gas accelerates more sharply through the throat compared to the N_2 case. This is because the speed of sound of the He gas at the throat, for example, is theoretically 2.7 times the N_2. The gas gradually accelerates after the throat until the separation point at $x \sim -20$ mm. The location of the NSW is at $x = 9$ mm, the same as the N_2 case. Although the 10 μm-Cu particle is accelerated more by He than N_2, the particle velocity relative to the gas velocity, at arbitrary x, is smaller for He than N_2.

The reason for the difference in the particle velocity for N_2 and He gases needs to be clarified to understand the gasdynamics of the cold spray. According to Eq 1, if we assume $u_p \ll u_g$, the gasdynamic drag force acting on the spray particle is approximately proportional to the momentum flux (MF); $\rho_g u_g^2$. However, according to the steady one-dimensional isentropic theory,

$$\frac{\left[\rho_g u_g^2\right]_{He}}{\left[\rho_g u_g^2\right]_{N_2}} = \frac{\left[\gamma / \left(1 + \frac{\gamma-1}{2} M_g^2\right)^{\frac{\gamma}{\gamma-1}}\right]_{He}}{\left[\gamma / \left(1 + \frac{\gamma-1}{2} M_g^2\right)^{\frac{\gamma}{\gamma-1}}\right]_{N_2}} \quad \text{(Eq 10)}$$

where, the specific heat ratio γ is 1.67 for He and 1.40 for N_2. The value of Eq 10 lies between 1.10 and 1.17 for $1.0 < M_g < 2.5$. The closeness of the values of MF for N_2 and He was also confirmed by the results of the CFD model, which is not shown here. Based on the discussion

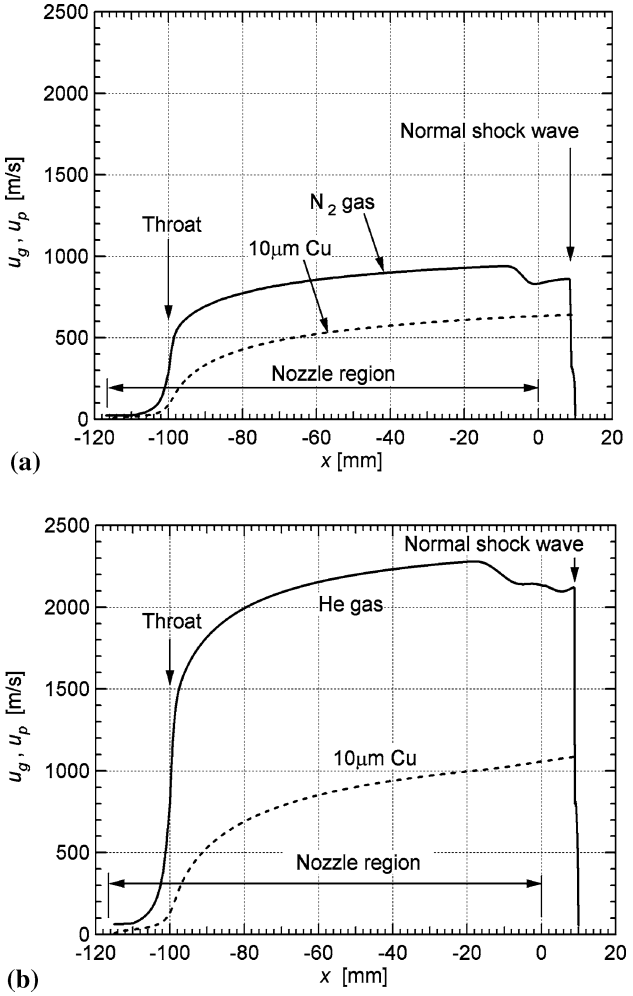

Fig. 3 Gas and 10 μm-Cu particle velocity on center line for (a) N_2, and (b) He

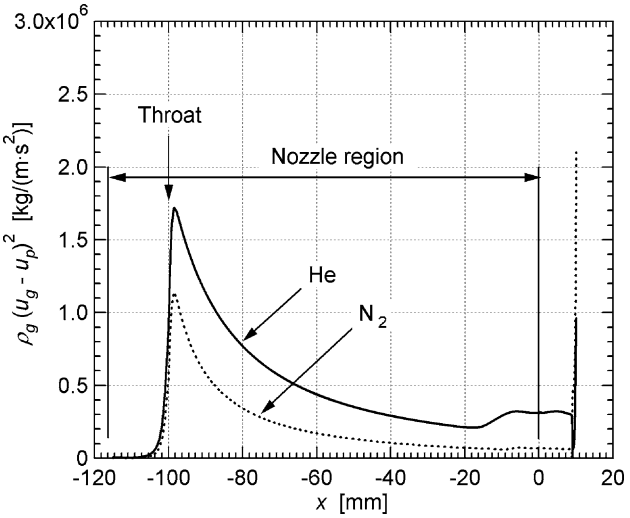

Fig. 4 Relative momentum flux for 10 μm-Cu particle on center line

made above, the assumption $u_p \ll u_g$ should not be used when considering the dependency of particle accelerating process on gas type.

When, we do not employ the assumption $u_p \ll u_g$, the gasdynamic drag force acting on the particle is proportional to the relative momentum flux (RMF); $\rho_g(u_g - u_p)^2$. Figure 4 shows the RMF on the center line for the 10 μm-Cu particle. It is clear that the difference of the RMF for He and N_2 is much larger than that of the theoretical MF along the horizontal axis. This means that the larger particle velocity propelled by He compared to N_2 is due to the larger RMF, not MF.

3.2 Particle Velocity and Temperature on Substrate

It is generally expected that the axial distributions of the simulated particle velocity u_p and temperature T_p differ from one powder-material to another. However, by investigating the equations of particle motion and temperature, we can see two parameters which are independent of the material type. The equation of particle motion, Eq 1, and that of particle temperature, Eq 3, can be modified as follows;

$$\frac{du_p}{dx} = \frac{3c_d\rho_g}{4u_p}(u_g - u_p)\cdot|u_g - u_p|\cdot\frac{1}{d_p\rho_p} \propto \frac{1}{d_p\rho_p} \qquad \text{(Eq 11)}$$

$$\frac{dT_p}{dx} = \frac{6k_{g,f}N_u(T_g - T_p)}{u_p}\cdot\frac{1}{d_p^2\rho_p C} \propto \frac{1}{d_p^2\rho_p C} \qquad \text{(Eq 12)}$$

Equation 11 shows that the combination parameter with respect to the particle $d_p\rho_p$, not d_p and ρ_p separately, affects the particle velocity. The parameter $d_p\rho_p$ is also pointed out by Jodoin (Ref 6), who calculated the velocity of particle flying through a NSW in cold spray. However, the parameter's usefulness in the non-uniform flow of the cold spray has not yet been fully verified. Hereafter, the product $d_p\rho_p$ is called particle-velocity-parameter (PVP) in this article. Likewise, Eq 12 indicates that the combination parameter with respect to the particle is $d_p^2\rho_p C$, which affects the particle temperature. The product $d_p^2\rho_p C$ is called particle-temperature-parameter (PTP) hereafter in this paper.

In Fig. 5, the particle velocity right before the NSW (open symbols) and particle impact velocity on the substrate, u_{pi} (solid symbols) on center line are plotted against the PVP for WC-12Co, Cu and Ti. The horizontal dash-dotted line shows the nozzle-exit gas velocity on the center line, u_{ge}, as a reference value. Figure 5(a) for N_2 shows that the particle velocity right before the NSW and that on the substrate are almost independent of the material type. It is also quite valuable to note in the figure that the maximum impact velocity, $u_{pi}^* = 735\,\text{m/s} = 735\,\text{m/s}$, is common for all three materials. (The asterisk as in u_{pi}^* shows the condition of the maximum impact velocity.) Furthermore, we can see in Fig. 5(a) that when the particle diameter is decreased, u_{pi}^* is obtained at the condition

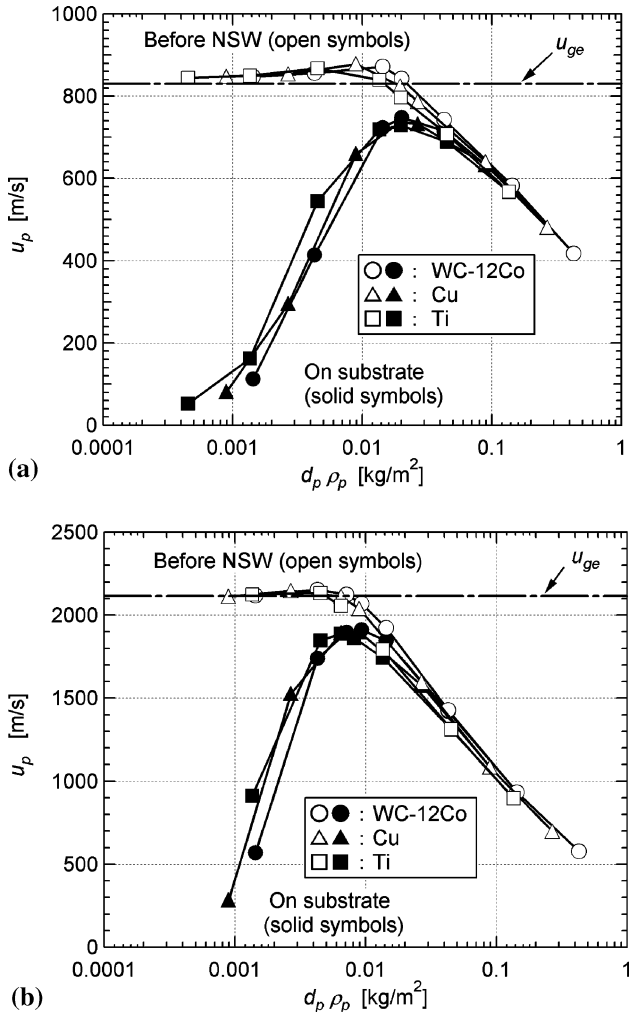

Fig. 5 Particle velocity vs. PVP for (a) N_2, and (b) He

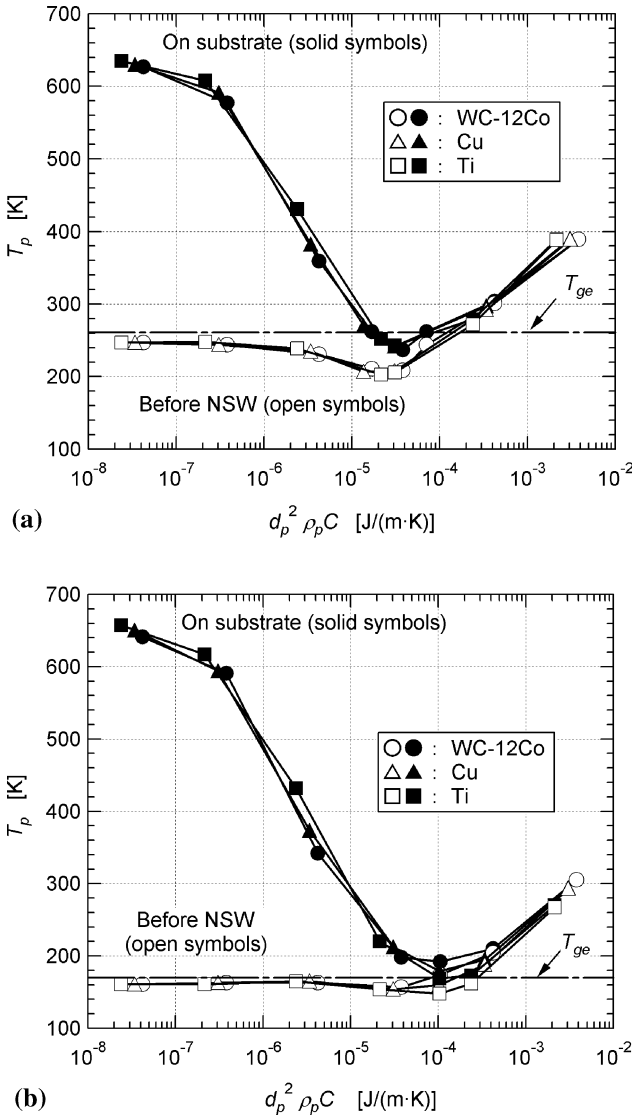

Fig. 6 Particle temperature vs. PTP for (a) N_2, and (b) He

that the particle-velocity right before the NSW first reaches the nozzle-exit gas velocity at

$$\text{PVP}^* \cong 0.020\,\text{kg/m}^2 \quad \text{for } N_2 \text{ at } u_{\text{pi}}^* = 735\,\text{m/s} \qquad \text{(Eq 13)}$$

For PVP < PVP*, the smaller the PVP, the smaller the particle impact velocity. The same trend can be observed in Fig. 5(b) for He. In the He case,

$$\text{PVP}^* \cong 0.0065\,\text{kg/m}^2 \quad \text{for He at } u_{\text{pi}}^* = 1900\,\text{m/s} \qquad \text{(Eq 14)}$$

where the particle velocity before the NSW reaches the gas velocity u_{ge}. The value of PVP* of He (0.0065 kg/m^2) is about one-third of that of N_2 (0.020 kg/m^2). This means that the NSW of He decelerates the particle less than the NSW of N_2.

In Fig. 6, the particle temperature right before the NSW (open symbols) and impact temperature on the substrate, T_{pi} (solid symbols) on the center line are plotted against PTP. The horizontal dash-dotted line in the figure shows the nozzle-exit gas temperature on the center line, T_{ge}.

Figure 6(a) for N_2 shows that the particle temperature before the NSW and that on the substrate are independent of the material type. In the range of PTP $> \sim 3\times10^{-5}$ J/(m K) of Fig. 6(a), the particle temperature before/after the NSW decreases with decreasing PTP. This trend can be explained qualitatively by using Eq 11 and 12, along with the gas temperature on the center line in the nozzle (not shown in this paper) as follows. The gas flow expands so rapidly after passing through the throat that the gas temperature is below the particle temperature from around the throat to the exit of the nozzle. The smaller particle has larger particle velocity; Eq 11 shows that du_{p}/dx is proportional to $1/d_{\text{p}}$, resulting in shorter residence time in the cooler supersonic gas flow. As for particle temperature, however, Eq 12 shows that dT_{p}/dx is proportional to $1/d_{\text{p}}^2$. As a result, smaller heat capacity dominates the particle temperature for smaller particles, instead of smaller residence time in the nozzle, in the

range of PTP $> \sim 3 \times 10^{-5}$ J/(m K). In addition, we can see in Fig. 6(a) that the particle temperature on the substrate increases for PTP $< \sim 3 \times 10^{-5}$ J/(m K). This is because the smaller particle has a smaller heat capacity, then the particle temperature easily follows the raised stagnant gas temperature on the substrate. The same trend can be seen in Fig. 6(b) of the He gas for PTP $< \sim 1 \times 10^{-4}$ J/(m K).

Finally, by using the results of Fig. 5 and 6, we can deduce the relationships between the maximum impact velocity u_{pi}^*, corresponding particle temperature T_{pi}^*, particle diameter d_p^*, and material properties of the particle as shown in Fig. 7. The graph consists of the partial fitting curves of solid symbols in Fig. 6, and curves of Eq 15 and 16 derived from Eq 13 and 14, respectively as;

$$d_p^* C \cong 0.020\left(C/\rho_p\right) \quad \text{for } N_2 \text{ at } u_{pi}^* = 735\,\text{m/s} \qquad \text{(Eq 15)}$$

$$d_p^* C \cong 0.0065\left(C/\rho_p\right) \quad \text{for He at } u_{pi}^* = 1900\,\text{m/s} \qquad \text{(Eq 16)}$$

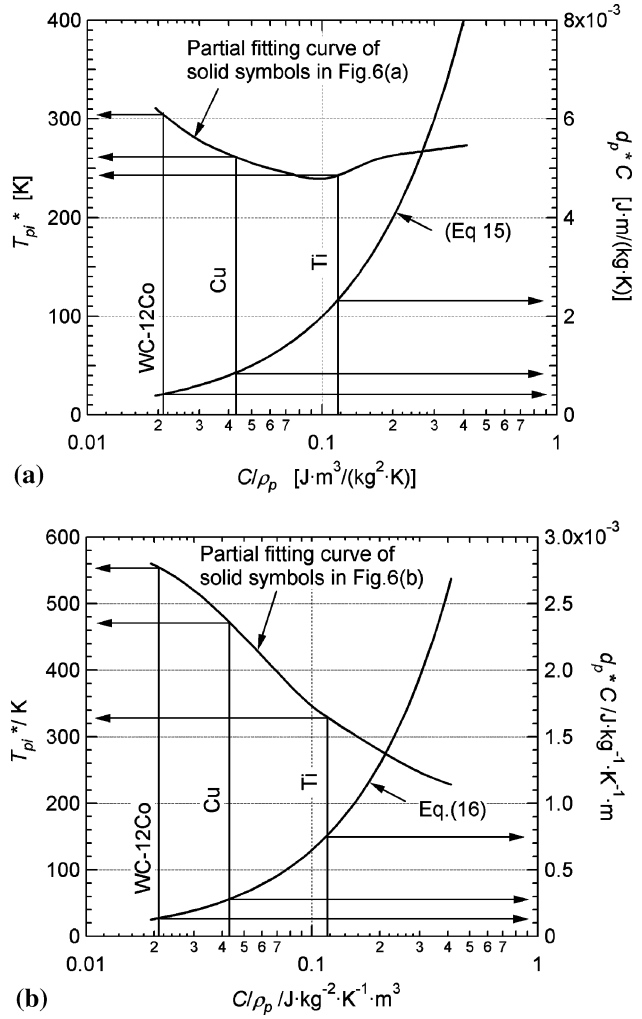

Fig. 7 Relationships between material properties, particle diameter, particle temperature for the maximum impact velocity of (a) 735 m/s for N_2 and (b) 1900 m/s for He

The horizontal axis of Fig. 7, C/ρ_p, is obtained from that of Fig. 6 by putting $d_p = d_p^*$, then $C/\rho_p = (d_p^{*2}\rho_p C)/(d_p^*\rho_p)^2 = (d_p^{*2}\rho_p C)/(\text{PVP}^*)^2$. The horizontal range of the curves in Fig. 7 was determined by considering a wide variety of the powder-materials normally used in the thermal spray process. Once the material type (value on the horizontal axis, C/ρ_p) is specified, T_{pi}^* and d_p^* are obtained from the left- and right-vertical axis of Fig. 7, respectively, to obtain u_{pi}^* of 735 m/s for N_2 in Fig. 7(a) and 1900 m/s for He in Fig. 7(b). Therefore, for the nozzle geometry shown in Fig. 2 and $p_{os} = 3$ MPa, $T_{os} = 572$ K, Fig. 7 can be used to estimate the conditions of the maximum impact-velocity for any powder-materials. In order to confirm this, the maximum impact-velocity condition of aluminium ($\rho_p = 2641$ kg/m^3, $C = 1040$ J/(kg·K)), which is not used to construct the curves in Fig. 7, is calculated for the He gas. Figure 7(b) yields $d_p^* = 2.65$ μm and $T_{pi}^* = 235$ K for Al, $C/\rho_p = 0.39$ J·m^3/(kg^2·K), to obtain $u_{pi}^* = 1900$ m/s. For comparison, the numerical integration of Eq 1 and 3 for $d_p = 2.65$ μm for the Al particle flying in the He gas flow obtained by CFD yield $u_{pi} = 1863$ m/s and $T_{pi} = 230$ K, respectively, which are almost identical to the graphical estimation from Fig. 7(b).

4. Concluding Remarks

The numerical simulation of the cold spray was performed to investigate the usefulness of the combination parameters, which are independent of the material type, that affect the particle velocity and temperature. A special attention was paid to the particle impact velocity. The N_2 and He were used as the process gas, respectively. The stagnation pressure and temperature of the gas upstream of the nozzle throat was set at 3 MPa and 576 K, respectively. The materials of the spray particle selected were WC-12Co, Cu and Ti. The particle-diameter range was 0.1-30 μm. The results are summarized as follows:

(1) The particle velocity right before the normal shock wave increases with decreasing the particle diameter until the particle velocity reaches the gas velocity at the nozzle exit at a specific particle diameter, where the impact velocity takes the maximum value. The maximum impact velocity is almost independent of the material type when the gasdynamic and geometrical spray conditions are fixed.

(2) The particle-diameter multiplied by the material density is the material-independent combination parameter, which affects the particle velocity. The maximum impact velocity is obtained for the combination-parameter of 0.020 kg/m^2 for nitrogen and that of 0.0065 kg/m^2 for helium, regardless of the material type.

(3) The squared particle-diameter multiplied by the material density and specific heat is the material-independent combination parameter which affects the particle temperature.

(4) The maximum impact velocity and corresponding particle temperature and diameter can be estimated

by using the two combination parameters for any powder-materials conventionally used in the thermal spray process.

References

1. T. Stoltenhoff, H. Kreye, and H.J. Richter, An Analysis of the Cold Spray Process and Its Coatings, *J. Thermal Spray Technol.*, 2002, **11**(4), p 542-550
2. T. Marrocco, D.G. McCartney, P.H. Shipway, and A.J. Sturgeon, Production of Titanium Deposits by Cold-Gas Dynamic Spray: Numerical Modeling and Experimental Characterization, *J. Thermal Spray Technol.*, 2006, **15**(2), p 263-272
3. M. Karimi, A. Fartaj, G. Rankin, D. Vanderzwet, W. Birtch, and J. Villafuerte, Numerical Simulation of the Cold Gas Dynamic Spray Process, *J. Thermal Spray Technol.*, 2006, **15**(4), p 518-523
4. W.-Y. Li and C.-J. Li, Optimal Design of a Novel Cold Spray Gun Nozzle at a Limited Space, *J. Thermal Spray Technol.*, 2005, **14**(3), p 391-396
5. R.C. Dykhuizen and R.A. Neiser, Optimizing the Cold Spray Process, *Thermal Spray 2003: Advancing the Science and Applying the Technology*, B.R. Marple and C. Moreau, Eds., May 5-8, 2003 (Orlando, FL, USA) ASM International, Materials Park, OH, 2003, p 19-26
6. B. Jodoin, Cold Spray Nozzle Mach Number Limitation, *J. Thermal Spray Technol.*, 2002, **11**(4), p 496-507
7. H.C. Yee, Upwind and Symmetric Shock-Capturing Schemes, NASA TM-89464, 1987, 127 pp
8. M.J. Zucrow and J.D. Hoffman, Gas Dynamics. John Wiley & Sons, NY, 1976, p 160-181
9. H.D. Kim, K. Matsuo, and T. Setoguchi, Investigation on Onset of Shock-Induced Separation, *Shock Waves*, 1996, **6**(5), p 275-286
10. A.B. Bailey and J. Hiatt, Sphere Drag Coefficient for a Broad Range of Mach and Reynolds Numbers, *AIAA J.*, 1972, **10**(11), p 1436-1440
11. Y.P. Wan, V. Prasad, G.-X. Wang, S. Sampath, and J.R. Fincke, Model and Powder Particle Heating, Melting, Resolidification, and Evaporation in Plasma Spraying Processes, *J. Heat Transfer*, 1999, **121**(3), p 691-699